https://doi.org/10.5194/egusphere-2025-12
Preprint. Discussion started: 23 January 2025

Direct assimilation of ground-based microwave radiometer observations with machine learning bias correction based on developments of RTTOV-gb v1.0 and WRFDA v4.5

Qing Zheng[1,3], Wei Sun[2,3], Zhiquan Liu[4], Jiajia Mao[5], Jieying He[6], Jian Li[2,3], Xingwen Jiang[1,3]

[1]Institute of Plateau Meteorology, China Meteorology Administration, Chengdu, 610213, China
[2]State Key Laboratory of Severe Weather, Chinese Academy of Meteorological Sciences, Beijing, 100081, China
[3]Institute of Tibetan Plateau Meteorology, China Meteorological Administration, Chengdu, 610213, China
[4]National Center for Atmospheric Research, Boulder, 80307-3000, USA
[5]Meteorological Observation Center, China Meteorological Administration, Beijing, 100081, China
[6]National Space Science Center, Chinese Academy of Sciences, Beijing, 100190, China

Correspondence to: Wei Sun (sunwei@cma.gov.cn)

Abstract. The application of ground-based microwave radiometers (MWRs), which provide high-quality and continuous vertical atmospheric observations, has traditionally focused on the indirect assimilation of retrieved profiles. This study advanced this application by developing a direct assimilation capability for MWR radiance observations within the Weather Research and Forecasting model data assimilation (WRFDA) system, along with a bias correction scheme based on random forest technique. The proposed bias correction scheme effectively reduced the observation-minus-background (O−B) biases and standard deviations by 0.83 K (97.1 %) and 1.63 K (64.6 %), respectively. A series of ten-day-long experiments demonstrated that assimilating MWR radiances improves both the initial conditions and the forecasts, with additional benefits from higher assimilation frequencies. In the initial conditions, hourly assimilation significantly enhanced low-level temperature and humidity fields, reducing the root-mean-square-error (RMSE) for temperature and water vapor mixing ratio by 6.32 % below 1 km and 1.98 % below 5 km. These improvements extended to forecasts, where 2 m temperature and humidity showed sustained benefits for over 12 hours, and precipitation forecasts exhibited notable gains, particularly for higher intensity events. The time-averaged Fractions Skill Score (FSS) for 3 h accumulated precipitation within the 24 h forecasts increased by 0.04–0.11 (10.2–58.1 %) for thresholds of 6–15 mm

1 Introduction

Data assimilation (DA), a core component of numerical weather prediction (NWP), plays an important role in improving the forecast accuracy by integrating observational data to refine initial conditions (Bauer et al., 2015; Gustafsson et al., 2018) Among various types of observations, microwave radiance data are crucial for DA due to their ability to penetrate the atmosphere and their sensitivity to temperature, humidity, clouds, and precipitation. Correspondingly, satellite-borne

https://doi.org/10.5194/egusphere-2025-12
Preprint. Discussion started: 23 January 2025

microwave radiance observations have been extensively studied and are considered among the most influential contributors to data assimilation systems (Geer et al., 2017; Kim et al., 2020; Candy and Migliorini, 2021)

Unlike satellite-borne radiometers, ground-based microwave radiometers (MWRs) offer unique advantages for DA, including high temporal resolution (minute-level) and greater sensitivity to the atmospheric boundary layer (ABL). Over the past two decades, the assimilation of MWRs has been increasingly studied, leading to improvements in the accuracy of NWP (Vandenberghe and Ware, 2002; Otkin, 2010; Hartung et al., 2011; Otkin et al., 2011; Caumont et al., 2016; HE et al., 2020; Qi et al., 2021, 2022; Lin et al., 2023). The assimilation of retrieved temperature and humidity profiles from MWRs has shown improvements in forecasting fog, storms, and precipitation. However, the reliance on indirect assimilation methods introduces uncertainties and complicates error quantification, which limits their overall effectiveness in enhancing forecast accuracy (Martinet et al., 2015; Caumont et al., 2016; Lin et al., 2023).

Direct assimilation of MWR radiances, which bypasses the retrieval process, offers significant advantages by avoiding retrieval-related errors and improving the effective use of observations. This approach requires accurate observation operators and robust bias correction to address differences between radiance observations and model states. The direct assimilation of satellite-borne radiance observations is relatively mature (Geer et al., 2008; Bauer et al., 2010; Geer et al., 2010; Eyre et al., 2020; Sun and Xu, 2021; Eyre et al., 2022) and utilizes fast radiative transfer models (RTMs) as observation-operator, such as Radiative Transfer for Television and Infrared Observation Satellite (Saunders et al., 2018). However, the unique characteristics of upward-looking MWR observations, such as sensitivity to near-surface conditions, require specialized RTMs and adaptation of existing techniques. It is noted that studies began to develop fast RTMs suitable for MWR, which provide a foundation for constructing observation operators for assimilation of MWR observations (De Angelis et al., 2016; Cimini et al., 2019; Shi et al., 2024). The RTTOV-gb, a ground-based version of the RTTOV model, was used to simulate brightness temperature from MWRs, demonstrating high accuracy (De Angelis et al., 2016, 2017; Cimini et al., 2019). Recent studies have demonstrated the potential of direct MWR radiance assimilation using RTTOV-gb to improve temperature, humidity, and precipitation forecasts (Cao et al., 2023; Vural et al., 2023).

Despite these advancements, previous studies have typically relied on limited MWR networks or focused on specific case studies. Additionally, research conducted in regions with relatively simple terrain may not fully address the complexities of areas like the Tibetan Plateau, where the presence of complex topography often leads to significant model biases (Yang et al., 2020; Wei et al., 2021). These biases make accurate bias correction essential for improving the effectiveness of direct assimilation, while traditional bias correction approach developed for satellite-borne microwave radiance observations are not directly applicable to ground-based MWRs.

To address these issues, this study integrates the RTTOV-gb into the Weather Research and Forecasting Data Assimilation (Barker et al., 2012) system to develop a direct assimilation module for MWR radiances. A nonlinear bias correction scheme based on machine learning is also constructed based on three months of observational data. The impact of direct MWR assimilation is then investigated through a series of ten-day experiments conducted in Southwest China, a region shaped by the influence of the Tibetan Plateau and characterized by complex terrain. The remainder of this paper is organized as follows.

https://doi.org/10.5194/egusphere-2025-12
Preprint. Discussion started: 23 January 2025

Section 2 describes the data, the implementation of RTTOV-gb in WRFDA, and the model configuration. Section 3 evaluates the performance of the bias correction scheme, followed by Sect. 4 presenting the impacts of MWR assimilation on the initial and forecast fields. The conclusions and discussion are presented in Sect. 5.

2 Methodology

2.1 Data

Two types of MWR sensors were assimilated in this study, as shown in Fig. 1: MP3000A and Humidity And Temperature Profiler (HATPRO). Atmospheric radiance is measured as brightness temperatures in 14 channels for HATPRO and 22 channels for MP3000A (Table 1). For HATPRO, channels 1–7 are in the K band, while channels 8–14 are in the V band. Similarly, for MP3000A, channels 1–8 are in the K band, and channels 9–22 are in the V band. The K band channels correspond to humidity-sensitive water vapor absorption lines, whereas the V band channels correspond to temperature-sensitive oxygen absorption lines.

The Fengyun-4B (FY-4B) Advanced Geosynchronous Radiation Imager (AGRI) cloud mask (CLM) is used to identify MWR-observed brightness temperatures under clear-sky conditions. The AGRI-based CLM product has a temporal resolution of 15 minutes and a horizontal resolution of 4 km, categorizing conditions as confidently cloudy, probably cloudy, probably clear, or confidently clear, with corresponding values of 0, 1, 2, and 3, respectively (Min et al., 2017). Due to its high quality, this cloud mask product is widely applied in satellite data assimilation (Yin et al., 2020, 2021; Xu et al., 2023; Shen et al., 2024).

The National Centers for Environmental Prediction (NCEP) Final Operational Global Analysis data (FNL) (0.25° × 0.25°, 6-hourly) were used to establish the initial and boundary conditions for regional NWP. Conventional observations from the Global Telecommunications System (GTS) were assimilated and evaluated, including land surface, marine surface, radiosonde, and aircraft reports. The hourly precipitation analysis product from the China Meteorological Administration Multisource Precipitation Analysis System (Shen et al., 2014) was used for evaluation. This dataset has been widely used in precipitation studies (Xia et al., 2019; Su et al., 2020; Sun and Xu, 2021; Wang et al., 2021; Li et al., 2023; Zheng et al., 2024)

Table 1. Central frequency for MWRs

Sensor	Frequencies for K band (GHz)	Frequencies for V band (GHz)
HATPRO	22.240;23.040;23.840;25.440; 26.240;27.840;31.400	51.260;52.280;53.860;54.940; 56.660;57.300;58.000
MP3000A	22.234;22.500;23.034;23.834; 25.000;26.234;28.000;30.000	51.248;51.760;52.280;52.804; 53.336;53.848;54.400;54.940; 55.500;56.020;56.660;57.288; 57.964;58.800

https://doi.org/10.5194/egusphere-2025-12
Preprint. Discussion started: 23 January 2025

2.2 Assimilation system and observation operator

The WRFDA system, developed by the National Center for Atmospheric Research (NCAR), is designed for data assimilation and includes three-dimensional variational (3DVAR), four-dimensional variational (4DVAR), and hybrid data assimilation algorithms. In this study, version 4.5 of the WRFDA system with 3DVAR is used for the direct assimilation of MWRs. The 3DVAR algorithm produces the analysis by minimizing a scalar objective cost function:

$$J(\boldsymbol{x}) = \frac{1}{2}(\boldsymbol{x}-\boldsymbol{x}_{\mathrm{b}})^{T}\mathbf{B}^{-1}(\boldsymbol{x}-\boldsymbol{x}_{\mathrm{b}}) + \frac{1}{2}(\boldsymbol{y}-\mathbf{H}(\boldsymbol{x}))^{\mathrm{T}}\mathbf{R}^{-1}(\boldsymbol{y}-\mathbf{H}(\boldsymbol{x}))\,, \quad (1)$$

where $\boldsymbol{x}$ and $\boldsymbol{x}_{\mathrm{b}}$ represents the analysis and background fields of the model variables, $\mathbf{y}$ is the vector of the observations, and $\mathbf{B}$ and $\mathbf{R}$ represent the background and observation error covariance matrices, respectively. The covariance matrix determines the weight assigned to the background and observations in the analysis, dictates how localized observation information is distributed vertically and horizontally in the model space, and maintains the balance among the model's control variables. $\mathbf{H}$ is the non-linear observation operator, that transforms model variables to the observed quantities. The observation operator works slightly differently for different types of observations. For conventional observations (e.g., temperature), the primary role of the observation operator is to perform spatiotemporal interpolation of model grid values to the observation space. For unconventional observations (e.g., reflectivity and radiance), where the model state cannot be directly compared with observations, the observation operator must also convert model variables into observed variables.

RTMs serve as observation operators for assimilating radiance data by mapping model variables (e.g., temperature and water vapor) into radiance space. RTTOV, a fast RTM, is widely used for assimilating satellite radiance data, which involves downward-looking observations. However, MWR radiances are upward-looking microwave observations, which differ from the downward-looking observation of satellites. This difference in direction makes RTTOV difficult to apply in MWR radiances assimilation. Fortunately, RTTOV-gb can simulate brightness temperatures from MWRs, and serves as the observation operator in this study. The weighting function (WF) quantifies the contribution of emissions from each atmospheric layer, and the maximum WF height indicates which atmospheric layer contributes most to the measured radiance (Carrier et al., 2008). The vertical distribution of WFs for HATPRO and MP3000A, calculated using RTTOV-gb, is shown in Fig. 2. The WFs reach their maximum at 1000 hPa and decrease monotonically with height. These results confirm that the lower atmosphere contributes most to the observed radiation across all channels, consistent with the findings of Shu et al. (2012).

It should be noted that RTTOV-gb is not included in the publicly available version of WRFDA. To address this limitation, an MWR direct assimilation module was developed, modeled after the satellite direct assimilation module, allowing RTTOV and RTTOV-gb to coexist within WRFDA. Results from the single-observation assimilation experiment confirm that the MWR direct assimilation module functions correctly. The temperature and water vapor increments are horizontally isotropic and show a maximum at lower atmospheric levels vertically (Fig. 2).

https://doi.org/10.5194/egusphere-2025-12
Preprint. Discussion started: 23 January 2025

2.3 Model configuration and experimental design

In this study, version 4.5 of the Weather Research and Forecasting (WRF) model (Skamarock et al., 2021) is used to simulate atmospheric evolution. The simulation employs a single domain (Fig. 1) with a horizontal resolution of 3 km, comprising 1,261 × 811 grid points and 51 vertical levels, with the top boundary at 10 hPa. The model physics configuration includes the Morrison two-moment microphysics scheme (Morrison et al., 2009), the Yonsei University PBL scheme (Hong et al., 2006), the Rapid Radiative Transfer Model for General Circulation Models (RRTMG) shortwave and longwave radiation schemes (Iacono et al., 2008), and the unified Noah land-surface model (Chen and Dudhia, 2001). Cumulus parameterization was excluded due to the convection-permitting horizontal resolution of 3 km (Li et al., 2023; Moker et al., 2018).

Based on the model configuration described above, four parallel experiments were conducted to investigate the impact of MWR assimilation (Table 2). Each experiment started at 12:00 UTC daily, incorporating 12 hours of data assimilation followed by a 24 h forecast. The primary differences among these experiments lie in the assimilated data and assimilation intervals. The CNTL experiment assimilated GTS data with a 6 h interval, while the MWR_6H experiment added MWR assimilation to the CNTL setup, enabling an evaluation of MWR assimilation's impact. The other two experiments, MWR_3H and MWR_1H, assimilated both GTS and MWR data with 3 h and 1 h intervals, respectively, to assess the effects of observation frequency in MWR assimilation. All experiments were conducted over a ten-day period from 13 October 2023 to 22 October 2023.

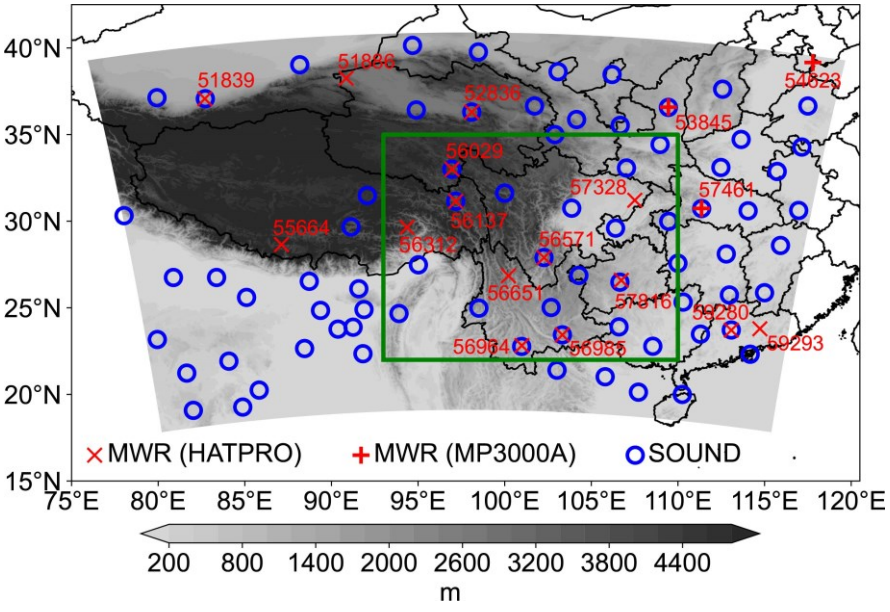

Figure 1: Computation domain(shaded). The shaded denotes topography (units: m). The green rectangle denotes the target region of Southwest China. The blue empty circle denotes radiosonde. The 'x' and '+' symbols denote HATPRO and MP3000A, respectively.

https://doi.org/10.5194/egusphere-2025-12
Preprint. Discussion started: 23 January 2025

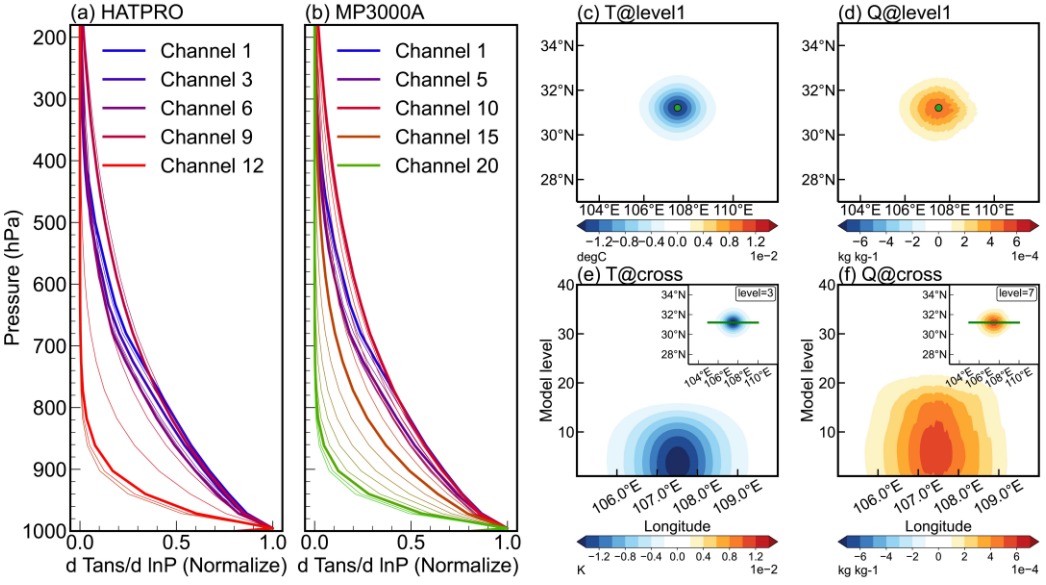

Figure 2: Weighting functions of (a) HATPRO and (b) MP3000A calculated by the RTTOV-gb. The (c, d) horizontal and (e, f) vertical analysis increments for (c, e) temperature and (d, f) water vapor mixing ratio in single-observation assimilation experiment. The main figures show vertical cross-sections of the increments along the green line shown in the inset figures. The inset figures show the horizontal increments at the model level with the maximum increment.

Table 2 Experimental design

Experiment	Assimilated Data	Assimilation Interval
CNTL	GTS	6-hour
MWR_6H	GTS and MWR	6-hour
MWR_3H	GTS and MWR	3-hour
MWR_1H	GTS and MWR	1-hour

3 Machine learning based bias correction for MWR

3.1 Bias characteristics

Variational assimilation assumes that both observation and background errors follow an unbiased Gaussian distribution. However, due to instrument errors, limitations of the RTMs, and errors in the NWP model background, observed radiances (O) and simulated radiances (B) inherently contain errors (denoted as μ^o and μ^b), which may exhibit a biased distribution. Bias correction is a crucial process in radiance data assimilation, aiming to identify and remove these biases (Auligné et al., 2007; Dee, 2005). In the real atmosphere, O and B are regarded as the true value (T) plus their respective deviations μ, as shown in Eq. (2):

https://doi.org/10.5194/egusphere-2025-12
Preprint. Discussion started: 23 January 2025

$$\overline{O-B} = \overline{(O-T)-(B-T)} = \overline{\mu^o - \mu^b}\,, \quad (2)$$

It shows the statistical expectation value of O−B can represent the systematic deviation ($\mu^o - \mu^b$) Therefore, it is critical to evaluate the bias characteristics of O−B and correct them.

To estimate the bias and develop a bias correction scheme for MWR direct assimilation, a three-month experiment was conducted to obtain a large number of samples. In this experiment, the WRF model was initialized every 6 hours using NCEP FNL data, and WRFDA operated hourly in monitoring mode (only calculate O−B). After a cloud check using AGRI-based CLM and gross check (O−B < 20 K), the bias of O−B for HATPRO and MP3000A was estimated.

Figure 3 shows the scatter of observed and simulated brightness temperatures for K band (water-vapor absorption lines) and V band (temperature-sensitive oxygen absorption lines). For HATPRO, more than 6,000 samples are analyzed. The O−B biases are 1.25 K for the K band (channel 1) and 2.14 K for the V band (channel 13), with standard deviations (STD) of 3.35 K and 2.82 K, respectively. Additionally, the scatter distribution of the V band is not centered, showing a band shifted to the right of the diagonal (Fig. 3b). For MP3000A, more than 2,000 samples are analyzed, with O−B biases of 3.06 K for the K band (channel 1) and −0.54 K for the V band (channel 14). The O−B STD are 3.94 K and 3.08 K, respectively. Similar to the HATPRO V band results, the scatter for the MP3000A V band also shows bands offset from the diagonal, but to the left (Fig. 3d). Based on the above results, the O−B STD of K band is larger than that of V band. Moreover, significant O−B biases are detected in MWR observations, with their characteristics varying across different sensors and channels. However, the correlation coefficients between observed and simulated brightness temperatures are high, at least 0.95, suggesting that these biases can be effectively corrected.

https://doi.org/10.5194/egusphere-2025-12
Preprint. Discussion started: 23 January 2025

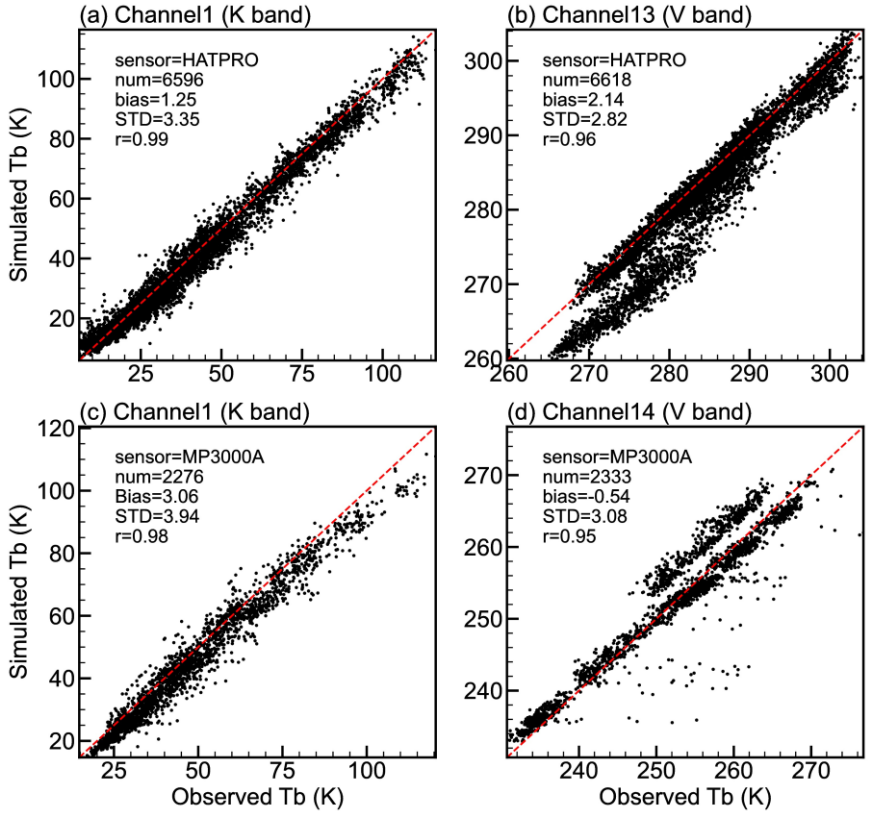

Figure 3: Scatter plot of observed brightness temperature (Tb) versus simulated Tb. The top and bottom rows correspond to the HATPRO and MP3000A sensors, and the left and right columns represent the K band and V band, respectively. Each panel displays the number of samples (num), the O−B mean (bias), O−B standard deviation (STD), and the correlation coefficient (r) between observed and simulated Tb.

To further analyze the O−B bias characteristics at each station and investigate the reasons for the band shifting from the diagonal (Fig. 3b and d), the statistics for each station are presented in Fig. 4. For HATPRO, the O−B bias varies among stations. Stations near complex topography (e.g., 56312, 56137, 56029, and 55664) exhibit notable positive O−B biases in channels 8 to 13 (Fig. 4a), leading to a rightward shift of the band relative to the diagonal (Fig. 3b). These positive biases may result from biases in the background field over the topographic region, the limited applicability of RTTOV-gb coefficients, or calibration issues in the observations. Consistent with results for all stations, each station shows that the O−B STD for the K band is larger than that for the V band (Fig. 4b). Regarding the correlation coefficients between observed and simulated brightness temperatures, the overall values are high but slightly lower for channels 4 to 9. For MP3000A, station 57461 exhibits a negative O−B bias in channels 9 to 14 (Fig. 4d), contributing to the band shifting to the left of the diagonal (Fig. 3d). Similar to the results for HATPRO, the O−B STD in the K band is generally larger than that in the V band (Fig. 4e), and the correlation coefficients are also overall higher, typically exceeding 0.9 (Fig. 4f).

https://doi.org/10.5194/egusphere-2025-12
Preprint. Discussion started: 23 January 2025

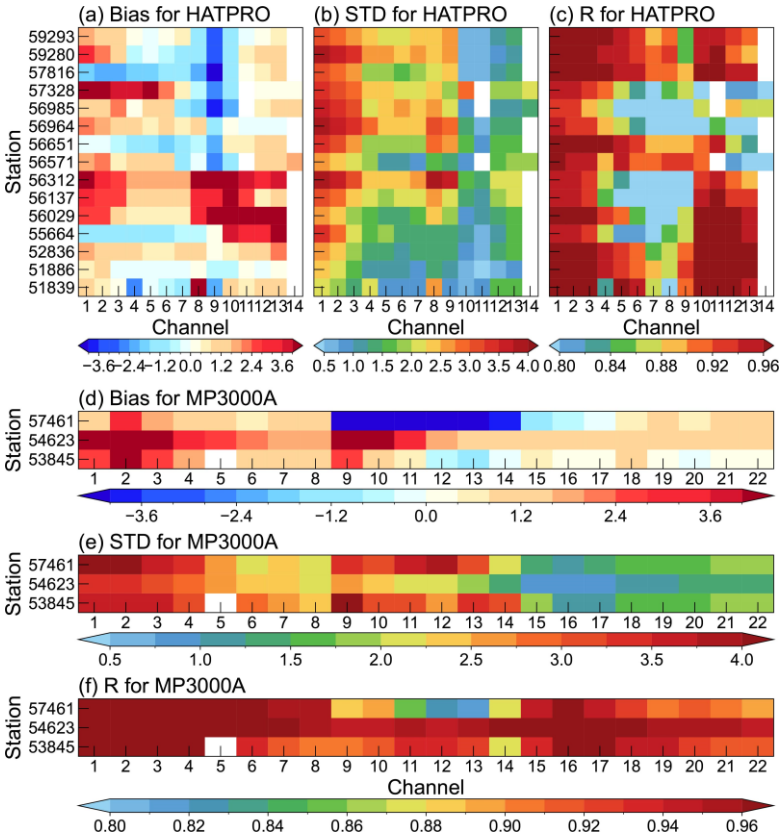

Figure 4: Statistics for each station. O−B (a) bias and (b) standard deviations (STD) for HATPRO; (c) correlation coefficient (r) between observed and simulated brightness temperatures for HATPRO; (d–f) same as (a–c) but for MP3000A.

3.2 Bias correction

Based on the results above, noticeable O−B biases were observed, varying across sensors, channels, and the geographical locations of stations. It is essential to remove these biases before assimilation. Static bias correction (Harris and Kelly, 2001) and variational bias correction (Dee, 2005) are commonly used in radiance data assimilation. These methods typically assume a linear correlation between the biases and some selected predictors. However, nonlinear sources of bias are common, and Zhang et al. (2023) demonstrated that the nonlinear scheme outperforms the linear scheme in reducing systematic biases. Following Zhang et al. (2023), this study developed a machine learning-based bias correction scheme, using the Random Forest (RF) technique (Breiman, 2001).

Following Yin et al. (2020), the predictors include 1,000–300hPa thickness, 200–50hPa thickness, model surface skin temperature (TS) and total precipitable water (PW). Considering that MWR are sensitive to the low-level atmosphere, the predictors also include 1,000–700hPa thickness, 700–500hPa thickness, 500–300hPa thickness, 2m temperature (T2), 2m water vapor mixing ratio (Q2), 10m zonal wind (U10), 10m meridional wind (V10), and surface pressure (PS). Finally, latitude, longitude, and observed brightness temperatures (Tb) are added as predictors due to their possible importance (Zhang et al.,

https://doi.org/10.5194/egusphere-2025-12
Preprint. Discussion started: 23 January 2025

2023). The O−B biases vary across sensors and channels. Therefore, a separate model is trained for each type of instrument and channel. Biases also vary across the geographical locations of stations, potentially influenced by the large-scale topography of the Tibetan Plateau. As predictors, 2 m temperature, surface pressure, and latitude and longitude are important for explaining these biases.

There are two types of parameters in machine learning models: model parameters and hyperparameters. Model parameters are initialized and updated during the learning process. Hyperparameters, on the other hand, cannot be directly estimated from the data. They must be configured before training because they define the model's architecture. Building an optimal machine learning model requires exploring a range of possibilities. The process of determining the ideal model architecture and hyperparameter configuration is known as hyperparameter tuning. This hyperparameter tuning is a key component of developing an effective machine learning model (Yang and Shami, 2020).

The RF model has four key hyperparameters: the number of trees in the forest (*n_estimators*), the maximum depth of the tree (*max_depth*), the minimum number of samples required to split an internal node (*min_samples_split*), and the minimum number of samples required to be at a leaf node (*min_samples_leaf*). These hyperparameters were tuned using GridSearchCV with 5-fold cross-validation (CV), which exhaustively searches over a predefined range of hyperparameters, training and evaluating the model for each configuration. The flowchart illustrating the training and evaluation process of the bias correction (BC) model is shown in Fig. 5b. The three-month dataset was split into a training set (70 %) and a test set (30 %). During training, GridSearchCV constructed a large grid of possible hyperparameter configurations, iteratively trained and evaluated the model for each, and calculated a score. Finally, the optimized model was trained using the configuration with the highest score.

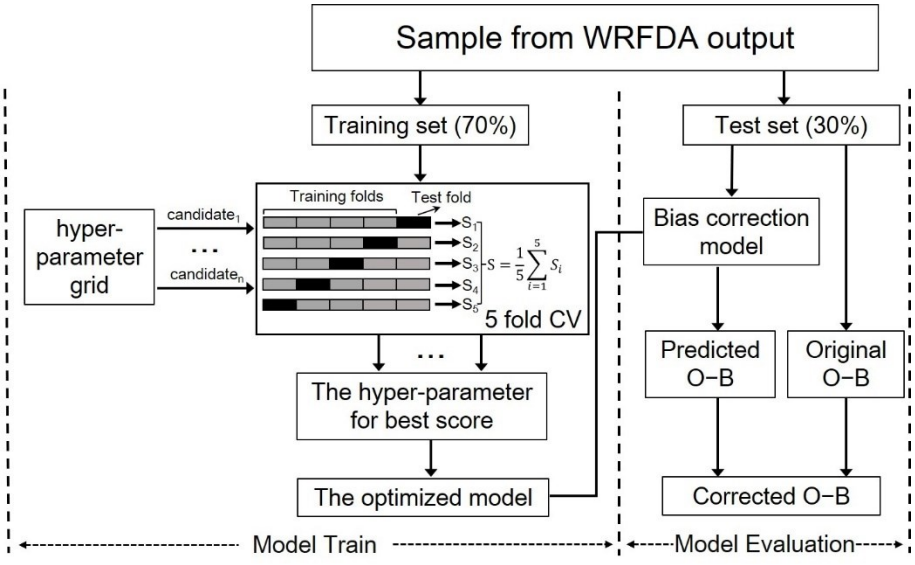

Figure 5: Flowchart of the training and evaluation for bias correction model

https://doi.org/10.5194/egusphere-2025-12
Preprint. Discussion started: 23 January 2025

To investigate the impact of hyperparameters on model training time and performance, the fit time and score of the RF model under various hyperparameter settings were analyzed (figure not shown). Overall, the fit time and score demonstrated a positive correlation. As the *min_samples_leaf* and *min_samples_split* parameters increased, both fit time and score decreased monotonically. Conversely, increasing the *max_depth* and *n_estimators* parameters resulted in a monotonic increase in both fit time and score. Notably, *max_depth* had the most significant impact on the score, while *n_estimators* primarily affected the fit time. For *n_estimators*, the score increased logarithmically, while the fit time grew linearly. These findings suggest that selecting a moderately small value for the *n_estimators* parameter can achieve better results while reducing computational time.

Using above bias correction model, the corrected O−B is obtained by subtracting the predicted O−B from the original O−B. The effectiveness of the BC model was assessed using the test set. The probability density function (PDF) of O−B for HATPRO was analyzed (figure not shown). Without BC, the O−B exhibits biases; for example, the PDF peak of channel 7 is located on the negative semi-axis, while the PDF peak of channel 13 is on the positive semi-axis. Furthermore, some individual channels, such as channel 10, display bimodal distributions. After bias correction, the PDF distributions approximate Gaussian distributions with a mean value of 0, indicating that the bias has been corrected. Figure 6 illustrates the bias and STD of the O−B for each HATPRO channel. Before BC, the bias of O−B for HATPRO ranged from 0 to 2 K, with the bias in the K band (particularly channels 4 to 7) being smaller than that in the V band. After bias correction, the bias for each channel is approximately 0 K. In terms of the O−B STD, the values for HATPRO ranged from 2 to 4 K without BC, with channels 4 to 7 exhibiting smaller values compared to other channels. After BC, the STD of O−B oscillates between 0.5 and 1.5 K. The application of this BC model significantly reduced both the bias and STD of O−B, with reductions of 0.83 K (97.1 %) and 1.63 K (64.6 %), respectively. Meanwhile, the corrected O−B distributions display Gaussian characteristics centered around zero, indicating the effective removal of systematic biases.

Diagnosing the contributions of each predictor is crucial. Figure 6c illustrates the feature importance of several predictors for HATPRO. The model normalized the feature importance scores so that their sum equals 1. A higher score reflects a stronger correlation between predictors and O−B biases. Observed brightness temperature, total precipitable water, and surface pressure are significant contributors to BC for the K band (water vapor channel). For the V band (temperature channel), observed brightness temperature, latitude, and surface pressure are the most influential predictors. The contributions of atmospheric thickness predictors are smaller compared to the other predictors; however, the 1,000–700 hPa thickness predictor has a relatively larger contribution among them. This may be because MWR primarily observes radiation from the lower atmosphere. Notably, surface pressure plays a critical role in BC for the temperature channels, which may account for the positive bias in O−B observed at plateau stations (Fig. 4a).

https://doi.org/10.5194/egusphere-2025-12
Preprint. Discussion started: 23 January 2025

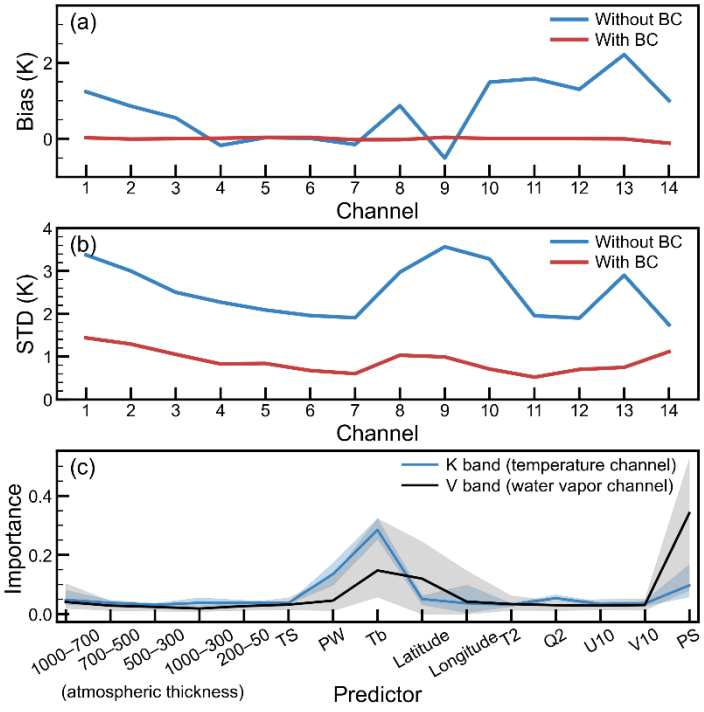

Figure 6: (a) Bias and (b) standard deviation (STD) of O−B. (c) Feature importance of the predictors used in the bias correction (BC) model. The shaded regions and solid lines represent the range and mean feature importance for the K band and V band, respectively.

4 Direct assimilation of MWR radiance observations

4.1 Assimilation impacts on initial condition

The performance of MWR assimilation in the observation space was evaluated. Figure 7 summarizes the bias and STD of the O−B and observation minus analysis (O−A) statistics, aggregated over time and across different channels. The bias of O−A was reduced compared to O−B, particularly in the V band. Specifically, for channel 11 of MWR_1H (1 h assimilation interval), O−B was −0.40 K and O−A was −0.13 K. When MWR observations were assimilated, the simulated brightness temperatures became closer to the observations, resulting in smaller STD. Moreover, as the frequency of MWR observation assimilation increases, the bias and STD of the O−B gradually converge closer to zero. For channel 3, the O−B STD in MWR_6H, MWR_3H, and MWR_1H significantly decreased from 1.03 K, 0.92 K, and 0.56 K to O−A STD values of 0.36 K, 0.34 K, and 0.34 K, respectively. Although the differences in O−A are less noticeable, the improvement of O−B suggests that increasing the frequency in cycling assimilation accumulates the impact of the MWRs, producing a higher-quality first-guess field for the final cycle. The assimilation of MWR observations effectively influences the brightness temperatures, demonstrating the successful processing of MWR data by the 3DVAR system.

https://doi.org/10.5194/egusphere-2025-12
Preprint. Discussion started: 23 January 2025

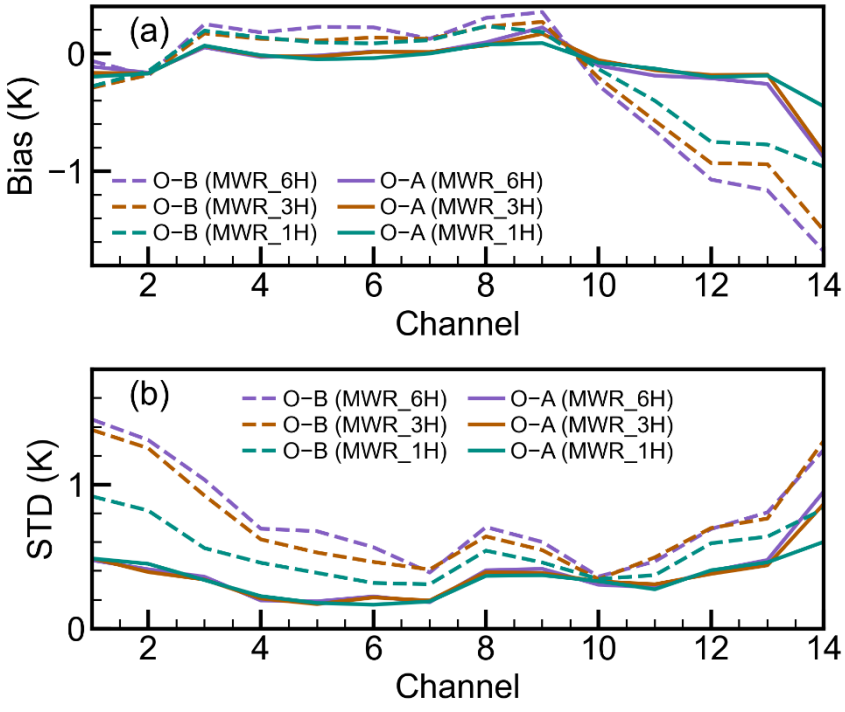

Figure 7: Verification of the initial condition against MWR observations in the target region of Southwest China (blue box in Fig. 1). (a) Bias and (b) standard deviation (STD) of the observation minus background (O−B) and observation minus analysis (O−A) for the MWR assimilation in the target region of Southwest China (blue box in Fig. 1).

The above evaluation demonstrates the successful implementation of the newly introduced MWR radiance direct assimilation in WRFDA. However, compared to brightness temperature simulations, greater attention should be given to the model state variables in the initial field, as they directly influence subsequent model forecasts. To this end, radiosonde observations in the target region of Southwest China were used to evaluate the impact of MWR assimilation. The root-mean-square error (RMSE) was calculated, and the RMSE differences between CNTL and other assimilation experiments are shown in Fig. 8.

Results indicate that assimilating MWR radiances enhances low-level temperature and humidity fields, with higher assimilation frequencies offering the potential for additional improvements. MWR assimilation has a neutral impact on atmospheric temperature above 1 km AGL, where the RMSE difference is minimal. However, it positively impacts lower atmospheric temperature, with the RMSE for temperature decreasing below 1 km AGL. Specifically, the average RMSE improvements below 1 km are 3.67 %, 5.28 %, and 6.32 % for MWR_6H, MWR_3H, and MWR_1H, respectively. This indicates that increasing assimilation frequency enhances observational impacts and further improves the initial field. The phenomenon becomes more pronounced with decreasing altitude, with 100 m RMSE improvements of 0.10 K (6.25 %), 0.13 K (7.90 %), and 0.19 K (11.34 %) in MWR_6H, MWR_3H, and MWR_1H, respectively. For the water vapor mixing ratio (QVAPOR), MWR assimilation demonstrates a positive impact that extends into the middle atmosphere, with average RMSE improvements below 5 km of 2.30 %, 2.20 %, and 1.98 % for MWR_6H, MWR_3H, and MWR_1H, respectively. The impact

https://doi.org/10.5194/egusphere-2025-12
Preprint. Discussion started: 23 January 2025

of MWR assimilation and the effect of assimilation frequency become more pronounced in the lower atmosphere, with average RMSE improvements below 300 m of 3.01 % for MWR_1H, compared to 2.43 % for MWR_6H and 2.05 % for MWR_3H. It is noted that the MWR assimilation shows limited improvement for the wind field. The RMSE for Zonal and Meridional winds exhibited a neutral impact when MWR was assimilated, with meridional winds even showing an increase in RMSE. The modest improvement in the wind field by MWR assimilation may be due to two factors: (1) When assimilating observed brightness temperature, the adjoint model of the observation operator directly adjusts temperature and humidity to optimize the simulation, while changes in the wind field are indirectly driven by these adjustments through the background error covariance. (2) MWR assimilation primarily improves the lower atmosphere, while changes in the upper atmosphere are also governed by the background error covariance. The static background error covariance used here is climatological and isotropic, which does not fully align with evolving weather conditions, potentially resulting in ineffective wind field improvements.

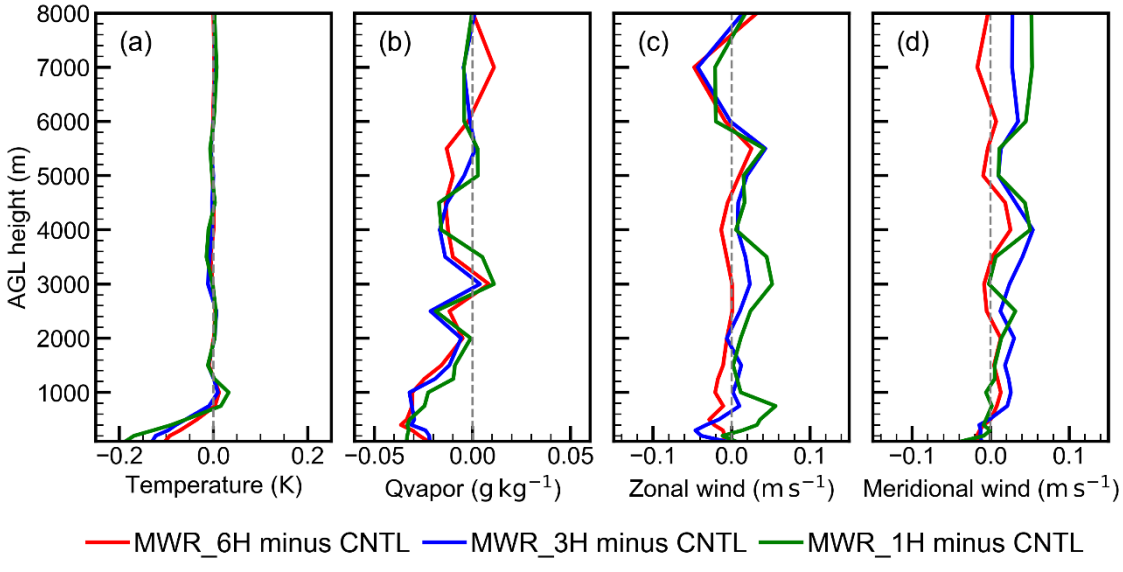

Figure 8: Verification of the initial condition against radiosonde observations in the target region of Southwest China (blue box in Fig. 1). Root mean square error (RMSE) for (a) temperature, (b) water vapor mixing ratio (QVAPOR), (c) zonal wind, and (d) meridional wind.

Based on the evaluation against radiosonde observations, the assimilation of MWR data improves the initial fields of temperature and humidity, aligning them more closely with observations, particularly in the lower atmosphere. Additionally, the initial fields are validated against station observations, including measurements of 2m temperature, 2m humidity, and 10m wind (Fig. 9).

The RMSE differences indicate that MWR assimilation effectively enhances the 2m temperature and humidity fields. Under 6-hourly MWR assimilation, the temperature RMSE generally increased on the southern side of the basin, whereas other regions showed a positive effect with reduced RMSE values. Moreover, the temperature RMSE reduction in these positively affected areas further improved as the assimilation frequency increased, with overall differences ranging from −0.008 K

https://doi.org/10.5194/egusphere-2025-12
Preprint. Discussion started: 23 January 2025

(−0.3 %) to −0.099 K (−4.1 %). For humidity, MWR assimilation shows a negative impact on relative humidity (RH) at a 6 h assimilation frequency. However, the RMSE over the plateau decreases as the assimilation frequency increases, with the RMSE difference shifting from positive to negative. In the MWR_1H experiment, the RH RMSE is reduced by 0.276 (1.3 %). Unlike the temperature and humidity RMSEs, the improvement in the wind field RMSE does not exhibit a distinct spatial pattern. Compared to the CNTL experiment, the RMSE differences for zonal wind are −0.005 m s^{-1} (−0.3 %), −0.017 m s^{-1} (−1.0 %), and −0.019 m s^{-1} (−1.2 %) in MWR_6H, MWR_3H, and MWR_1H, respectively. Similarly, the RMSE differences for meridional wind are −0.008 m s^{-1} (−0.5 %), −0.011 m s^{-1} (−0.7 %), and −0.009 m s^{-1} (−0.5 %) in MWR_6H, MWR_3H, and MWR_1H, respectively. While the changes in wind RMSE are relatively small, the results indicate that assimilating MWR data improves the initial field, with higher assimilation frequencies offering potential for further enhancement.

https://doi.org/10.5194/egusphere-2025-12
Preprint. Discussion started: 23 January 2025

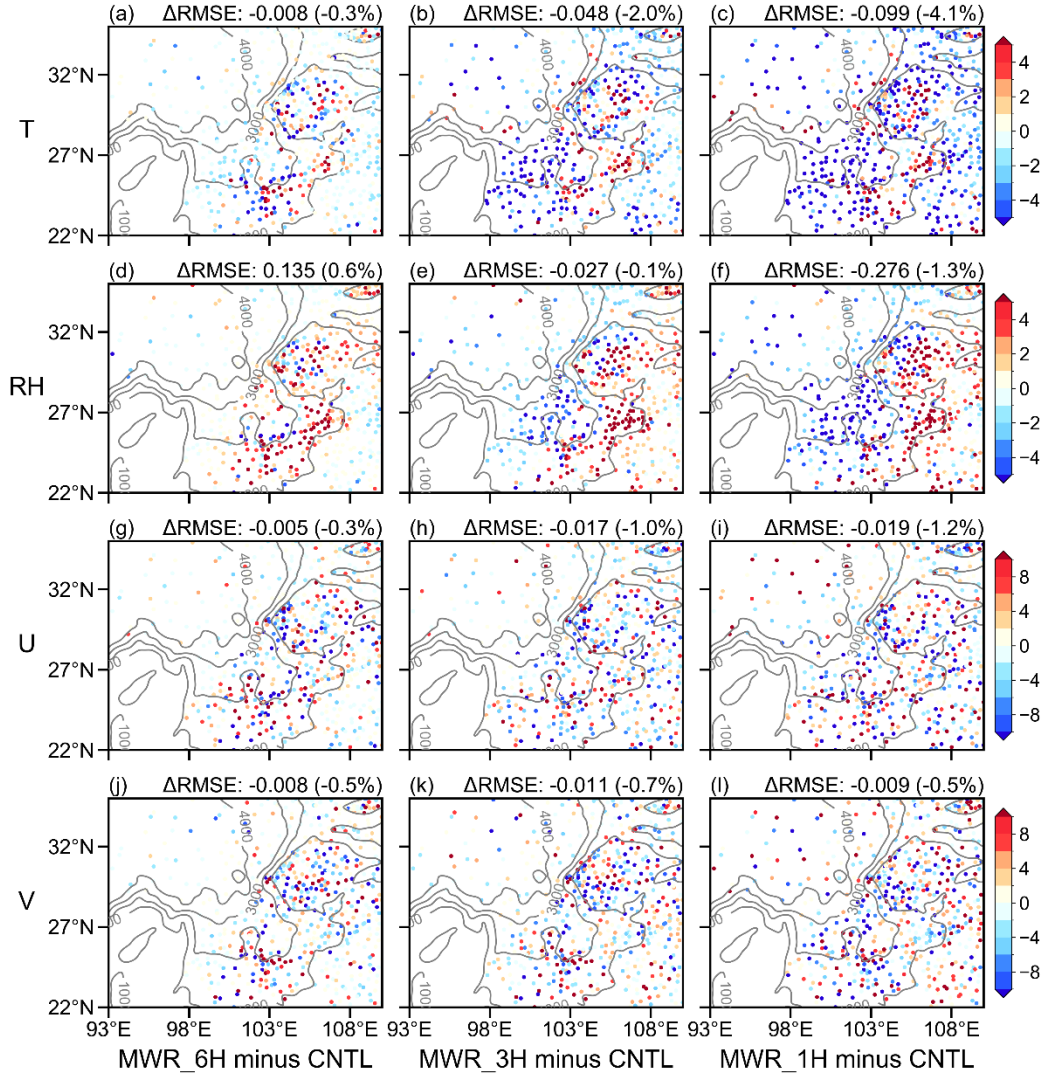

Figure 9: Verification of the initial condition against station observations in the target region of Southwest China (blue box in Fig. 1). The percentage in RMSE differences (scatter) for temperature (T), relative humidity (RH), zonal wind (U), and meridional wind (V). The grey solid line is the topography height (m).

4.2 Assimilation impacts on forecast field

After presenting the improvements in the initial condition, this section investigate the impact of MWR assimilation on the 24 h forecasts. The time series of RMSE differences (assimilation experiments minus the CNTL experiment) against station observations for 2 m temperature, 2 m relative humidity, and 10 m wind fields are shown in Fig. 10. For temperature, the negative RMSE difference gradually increases, approaching zero at a lead time of 6 hours, with higher assimilation frequency (MWR_1H) achieving a greater RMSE reduction. Similar results are observed for relative humidity, where the RMSE difference also increases and approaches zero at a lead time of 12 hours. MWR_1H consistently demonstrates the largest

https://doi.org/10.5194/egusphere-2025-12
Preprint. Discussion started: 23 January 2025

RMSE reduction for relative humidity. For the wind field, no increase in the RMSE difference with lead time was observed, as previously described. However, the RMSE differences between the assimilation experiments and the CNTL experiment remain overall negative, indicating that MWR assimilation improves wind forecasts. Additionally, MWR_1H demonstrates the largest RMSE reduction in meridional wind, suggesting that increasing the frequency of MWR assimilation may lead to further improvements. The quantitative statistics are presented in Table 3. The temperature RMSE differences between MWR_6H and CNTL are −0.012, −0.005, and −0.004 K for lead time of 1–6 hours, 1–12 hours, and 1–24 hours, respectively. This gradual decrease in RMSE difference with increasing forecast time is also observed in other experiments and variables, indicating a weakening of the positive impact of MWR assimilation as the forecast period extends, likely due to a gradual increase in model error. When the impact of MWR assimilation is most pronounced (at a lead time of 1–6 hours), the temperature RMSE differences range from −0.012 K in MWR_6H to −0.019 K in MWR_3H, and −0.030 K in MWR_1H. The temperature RMSE reduction increases with the frequency of MWR assimilation, a trend also observed in relative humidity and wind, suggesting that increasing the assimilation frequency can further improve forecasts. Although these differences are small, the results reflect the potential for improved model forecasts with MWR assimilation.

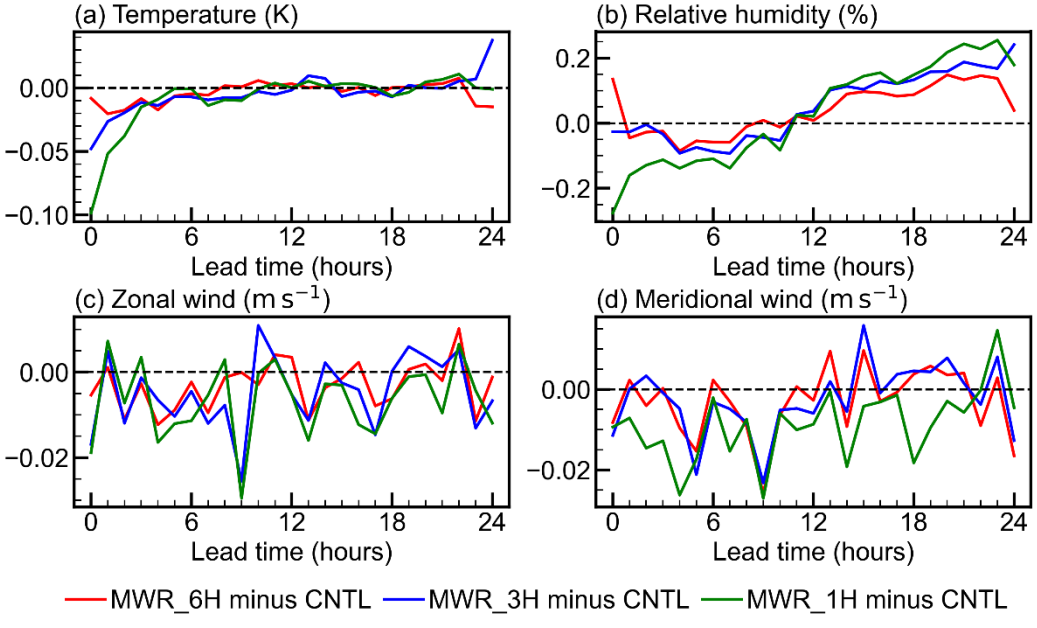

Figure 10: Verification of the forecast against station observations. RMSE differences for (a) temperature, (b) relative humidity, (c)zonal wind, and (d) meridional wind between the assimilation experiments and the CNTL experiment.

https://doi.org/10.5194/egusphere-2025-12
Preprint. Discussion started: 23 January 2025

Table 3 RMSE difference against station observations.

EXP	Lead time (hour)	Temperature (K)	Relative Humidity (%)	Zonal wind ($m\ s^{-1}$)	Meridional wind ($m\ s^{-1}$)
MWR_6H minus CNTL	1–6	−0.012	−0.011	−0.006	−0.005
	1–12	−0.005	−0.027	−0.003	−0.006
	1–24	−0.004	0.046	−0.003	−0.003
MWR_3H minus CNTL	1–6	−0.019	−0.042	−0.007	−0.006
	1–12	−0.010	−0.036	−0.006	−0.007
	1–24	−0.003	0.072	−0.005	−0.003
MWR_1H minus CNTL	1–6	−0.030	−0.153	−0.008	−0.013
	1–12	−0.012	−0.087	−0.006	−0.013
	1–24	−0.005	0.065	−0.006	−0.009

Verification against station observations indicate that assimilating MWR radiances improves near-surface forecasts, with higher assimilation frequencies offering potential for further enhancement. To further examine the impact of MWR assimilation, Fig. 11 presents the forecast verification against radiosonde measurements. Unlike the RMSE differences for the initial condition (Fig. 8), the MWR assimilation did not reduce the RMSE for lower atmospheric temperature and water vapor mixing ratio, indicating a neutral impact of MWR assimilation on forecasts. Similarly, the wind field verification results did not show significant improvements with MWR assimilation. While the RMSE of zonal wind was reduced in the MWR_1H experiment, the RMSE differences for the wind field in other experiments were close to or greater than zero, suggesting a neutral to slightly negative impact of MWR assimilation on wind forecasting. According to the verifications against radiosonde data, limited improvements are found in the forecasts through MWR assimilation. This may be attributed to increased model error with longer lead time, reducing the effectiveness of initial condition improvements from MWR assimilation. It should be noted that 12 h and 24 h forecast fields were verified against radiosonde data. Moreover, verification against station observations indicates that temperature improvements were primarily concentrated within the first 6 hours, while humidity improvements extended to the first 12 hours.

https://doi.org/10.5194/egusphere-2025-12
Preprint. Discussion started: 23 January 2025

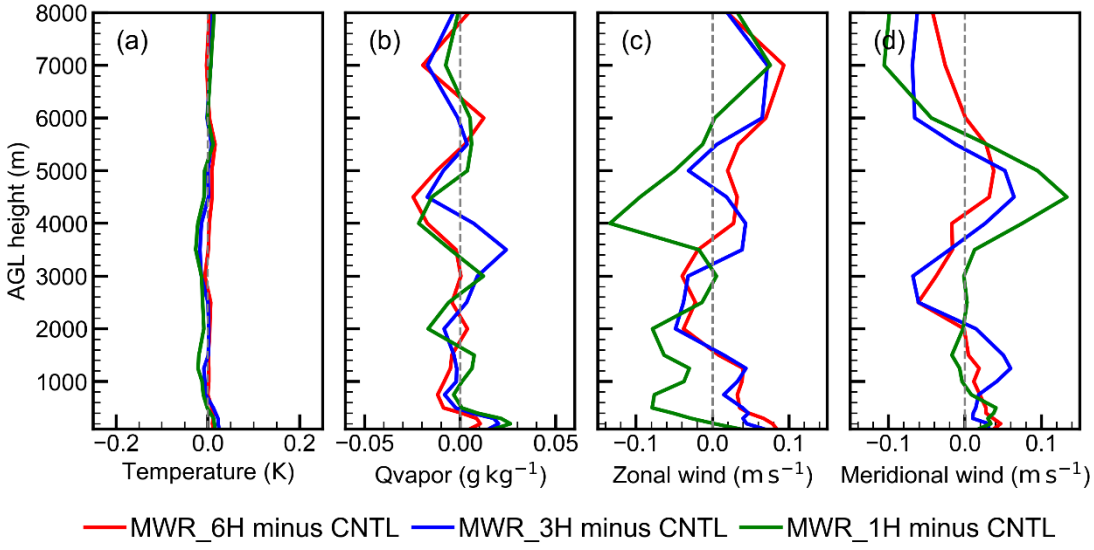

Figure 11: Same as Fig. 8, but for forecast at lead time of 12 and 24 hours.

370 To further explore the role of MWR assimilation in precipitation forecasting, the fractions skill score (FSS) of 3 h accumulated precipitation forecasts was calculated. The radius of influence for the FSS was set to 18 km, equivalent to six times the grid spacing (Ha and Snyder, 2014; Zheng et al., 2024). Figure 12 presents the time series of FSS differences between the assimilation experiments and the CNTL experiment. The results indicate that assimilating MWR radiances improves precipitation forecasting, with FSS differences increasing progressively with higher precipitation intensities. Additionally, 375 increasing assimilation frequencies shows the potential to further enhance forecast performance. When assimilating MWR data at a 1 h frequency, the time-averaged FSS improvements for 3 h accumulated precipitation are 0.04 (10.2 %) for the 6 mm threshold, 0.08 (23.5 %) for 9 mm threshold, 0.11 (40.8 %) for 12 mm threshold, and 0.11 (58.1 %) for 15 mm threshold precipitation. For 3 h accumulated precipitation with a threshold of 15 mm, the time-averaged FSS improvements are 0.03, 0.06, and 0.11 for MWR_6H, MWR_3H, and MWR_1H, respectively. These findings are consistent with the above 380 verification against radiosonde and station observations, suggesting that MWR assimilation can improve forecasts and that higher-frequency assimilation leads to further enhancements.

https://doi.org/10.5194/egusphere-2025-12
Preprint. Discussion started: 23 January 2025

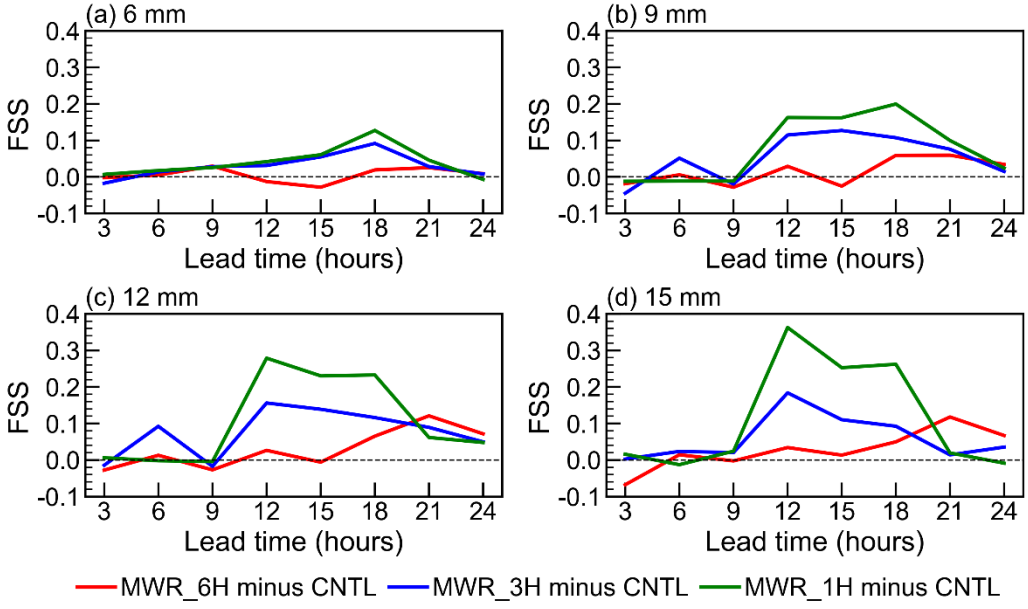

Figure 12: The time series of fractions skill score (FSS) differences (assimilation experiments minus the CNTL experiment). The FSS was calculated for 3 h accumulated precipitation for thresholds of (a) 6 mm, (b) 9 mm, (c) 12 mm, and (d) 15 mm.

5 Conclusions and Discussion

To investigate the impact of directly assimilating MWRs in Southwest China, MWR assimilation module is built in WRFDA-4.5, where RTTOV-gb is used as observation operator. Based on this module, three-month O−B statistic sample was calculated to evaluate the bias for O−B and develop a BC model. Furthermore, 10-days assimilation experiments (Table 2) using this MWR assimilation module and BC model are conducted to investigate the impact of the direct assimilation MWR and the effects of assimilation frequency. The main findings are as follows:

1.Based on three months of hourly samples, noticeable O−B biases were observed, varying across sensors, channels, and geographical locations. The machine learning-based bias correction scheme, employing a RF model, effectively reduced these systematic biases. After applying this BC model, both the bias and STD of the O−B were substantially reduced. Specifically, the bias and STD decreased by 0.83 K (97.1 %) and 1.63 K (64.6 %), respectively. The corrected O−B distributions exhibited Gaussian characteristics centered around zero, indicating the successful mitigation of systematic biases.

2.Assimilating MWR enhances the accuracy of initial atmospheric conditions, with higher assimilation frequencies amplifying the positive impact, particularly for temperature and humidity in the lower atmosphere. Evaluation against radiosonde observations shows that the temperature RMSE below 1 km AGL decreases by 3.67 % to 6.32 %, with improvements below 100 m AGL ranging from 6.25 % to 11.34 % for 6 h, 3 h, and 1 h assimilation frequencies, respectively. For the water vapor mixing ratio, positive impacts extend up to 5 km AGL, with average RMSE improvements ranging from 1.98 % to 2.30 %.

https://doi.org/10.5194/egusphere-2025-12
Preprint. Discussion started: 23 January 2025

Verification against station observations further supports these findings, indicating that the RMSE for 2 m temperature decreases by up to 4.1 %, while the RMSE for 2 m relative humidity decreases by up to 1.3 % at the 1 h assimilation frequency. 3. The assimilation of MWR observations leads to improvements in forecasts, and increasing assimilation frequencies has potential to get further improvement. In the first 6 hours of the forecast, the temperature RMSE decrease by 0.012 K, 0.019 K, and 0.030 K with 6 h, 3 h and 1 h MWR assimilation frequency, respectively. Similar trends are observed for relative humidity, the experiment with 1 h MWR assimilation frequency showing the largest decrease in RMSE. MWR assimilation also improves precipitation forecasts, with further enhancements seen as assimilation frequency increases. For 1 h MWR assimilation, time-averaged FSS improvements reach 0.04 for the 6 mm threshold, 0.08 for 9 mm, and 0.11 for both 12 mm and 15 mm thresholds. In the three-month O−B statistics, the STD in the K band is larger than that in the V band, consistent with the findings of (Vural et al., 2023) and (Cao et al., 2023). This phenomenon may be attributed to the K-band's sensitivity to water vapor and the V-band's sensitivity to temperature, with model temperature accuracy being better than that of water vapor. The O−B bias varies across sensors, channels, and geographical locations, with a notable positive bias observed at high-altitude stations. This positive bias is potentially caused by large-scale topographical effects on the Tibetan Plateau, where model simulations may introduce errors, and RTTOV-gb coefficients may be inapplicable. The RTTOV-gb coefficient files are trained on global profiles and are not tailored to the plateau region; consequently, their vertical coordinates extend up to 1050 hPa, while surface pressure in the plateau region typically exceeds 700 hPa.

A machine learning-based bias correction scheme using the RF technique was developed, demonstrating strong performance. The number of trees is a critical hyperparameter that must be predetermined. Training time increases linearly with the number of trees, while performance gradually plateaus. Thus, a modest number of trees, such as 50, can balance efficiency and accuracy. Feature importance analysis for BC predictors revealed observed brightness temperature, atmospheric precipitable water, and surface pressure as key factors for correcting biases. The importance of brightness temperatures aligns with findings in satellite data bias correction(Liu et al., 2022; Zhang et al., 2023). Atmospheric precipitable water is essential for the K band, a humidity-sensitive channel. Surface pressure plays a key role in temperature channels, thereby accounting for the positive bias observed in plateau regions. Although atmospheric thickness predictors contributed less overall, the 1,000–700 hPa thickness was relatively significant, likely due to MWRs primarily sensing radiation from the lower atmosphere.

In this study, direct assimilating MWR radiance enhances both the initial conditions and the forecasts, show a great potential in improving ABL and precipitation simulations. However, as a preliminary attempt, it is admitted that the study has some limitations. Firstly, only static background-error covariances were used in this study. The background error covariance matrix plays an important role in variational data assimilation, and this type covariances are climatological, spatially homogeneous, and isotropic. This may limit the impact of MWR assimilation, and flow-dependent error covariances should be implemented in the future work. Second, only clear-sky MWRs were assimilated in this study. Since precipitation processes are often accompanied by extensive cloud cover, few clear-sky MWRs were available. To better explore the potential of MWR assimilation, experiments focused on periods with abundant clear-sky MWRs, which coincided with minimal heavy precipitation. Studies on satellite all-sky assimilation show that including cloud- and precipitation-affected data improves

https://doi.org/10.5194/egusphere-2025-12
Preprint. Discussion started: 23 January 2025

forecasts(Ma et al., 2022; Xian et al., 2019), highlighting the need for future research on all-sky assimilation of MWRs. It is noted that satellite-based microwave radiometers are primarily sensitive to the middle and upper atmosphere, while ground-based MWRs provide valuable observations of the lower atmosphere (Shi et al., 2023).Building on this study, future research could explore the joint direct assimilation of satellite-based and ground-based microwave radiometers. By leveraging their complementary observational capabilities, this approach has the potential to further enhance the accuracy of atmospheric analysis and improve forecasting across multiple layers of the atmosphere.

Code availability

The original RTTOV-gb v1.0 can be obtained via the request form on the NWPSAF website (https://nwp-saf.eumetsat.int/site/software/rttov-gb/). The WRF v4.5 and WRFDA v4.5 are open-source models and can be downloaded from https://github.com/wrf-model/WRF. Due to the ongoing operational testing of this technology and the licensing restrictions of RTTOV-gb, the developed versions of RTTOV-gb and WRFDA can be requested by contacting the corresponding author (sunwei@cma.gov.cn) or Qing Zheng (zq551379@outlook.com). Additionally, the code for training the machine learning-based MWR bias correction model is available on Zenodo (https://doi.org/10.5281/zenodo.14586317; Zheng et al., 2025a)

Data availability

The MWR data and precipitation analysis product are provided by the Chinese Meteorological Administration and can be obtained via request from https://www.cma.gov.cn/en/. The AGRI CLM used are available at https://satellite.nsmc.org.cn/portalsite/default.aspx?currentculture=en-US. The NCEP FNL data used are available at https://rda.ucar.edu/datasets/d083003/. The assimilated GTS data are available at https://rda.ucar.edu/datasets/d337000/. The model outputs for the single-observation assimilation experiment and the three-month sample data for the "Machine learning based bias correction for MWR" section is available on Zenodo (https://doi.org/10.5281/zenodo.14586346; Zheng et al., 2025b)

Author contribution

WS conceived the idea and designed the research. QZ performed the research and wrote the first draft of the manuscript. All authors discussed the results and contributed to writing and revisions.

Competing interests

The authors declare no conflicts of interest or competing financial interests.

https://doi.org/10.5194/egusphere-2025-12
Preprint. Discussion started: 23 January 2025

Acknowledgements

The authors gratefully acknowledge Dr. Domenico Cimini for his help in usage of RTTOV-gb. They also thank the Numerical Weather Prediction Satellite Application Facility (NWP SAF) for providing the source code of RTTOV-gb v1.0, and the National Center for Atmospheric Research (NCAR) for providing the source code of WRF v4.5 and WRFDA v4.5. Additionally, the authors appreciate the National Centers for Environmental Prediction (NCEP) for providing the FNL data, the China Meteorological Administration (CMA) for supplying the MWR data and precipitation analysis product, and the National Supercomputing Center in Chengdu for their computational support.

Financial support

This study was jointly supported by the National Key Research and Development Program of China (2023YFC3007504), the National Natural Science Foundation of China (42475013), Sichuan Science and Technology Program (2024YFFK0110) Southwest Sichuan (Ya'an) Rainstorm Laboratory (CXNBYSYSZD202401).

References

Auligné, T., McNally, A. P., and Dee, D. P.: Adaptive bias correction for satellite data in a numerical weather prediction system, Quarterly Journal of the Royal Meteorological Society, 133, 631–642, https://doi.org/10.1002/qj.56, 2007.

Barker, D., Huang, X.-Y., Liu, Z., Auligné, T., Zhang, X., Rugg, S., Ajjaji, R., Bourgeois, A., Bray, J., Chen, Y., Demirtas, M., Guo, Y.-R., Henderson, T., Huang, W., Lin, H.-C., Michalakes, J., Rizvi, S., and Zhang, X.: The Weather Research and Forecasting Model's Community Variational/Ensemble Data Assimilation System: WRFDA, Bulletin of the American Meteorological Society, 93, 831–843, https://doi.org/10.1175/BAMS-D-11-00167.1, 2012.

Bauer, P., Geer, A. J., Lopez, P., and Salmond, D.: Direct 4D-Var assimilation of all-sky radiances. Part I: Implementation, Quarterly Journal of the Royal Meteorological Society, 136, 1868–1885, https://doi.org/10.1002/qj.659, 2010.

Bauer, P., Thorpe, A., and Brunet, G.: The quiet revolution of numerical weather prediction, Nature, 525, 47–55, https://doi.org/10.1038/nature14956, 2015.

Bormann, N., H. Lawrence and J. Farnan, 2019: Global observing system experiments in the ECMWF assimilation system, ECMWF Tech. Memo, 839, 23pp.

Breiman, L.: Random Forests, Machine Learning, 45, 5–32, https://doi.org/10.1023/A:1010933404324, 2001.

Candy, B. and Migliorini, S.: The assimilation of microwave humidity sounder observations in all-sky conditions, Quarterly Journal of the Royal Meteorological Society, 147, 3049–3066, https://doi.org/10.1002/qj.4115, 2021.

Cao, Y., Shi, B., Zhao, X., Yang, T., and Min, J.: Direct Assimilation of Ground-Based Microwave Radiometer Clear-Sky Radiance Data and Its Impact on the Forecast of Heavy Rainfall, Remote Sensing, 15, 4314, https://doi.org/10.3390/rs15174314, 2023.

https://doi.org/10.5194/egusphere-2025-12
Preprint. Discussion started: 23 January 2025

Carrier, M. J., Zou, X., and Lapenta, W. M.: Comparing the Vertical Structures of Weighting Functions and Adjoint Sensitivity of Radiance and Verifying Mesoscale Forecasts Using AIRS Radiance Observations, Monthly Weather Review, 136, 1327–1348, https://doi.org/10.1175/2007MWR2057.1, 2008.

Caumont, O., Cimini, D., Löhnert, U., Alados-Arboledas, L., Bleisch, R., Buffa, F., Ferrario, M. E., Haefele, A., Huet, T., Madonna, F., and Pace, G.: Assimilation of humidity and temperature observations retrieved from ground-based microwave radiometers into a convective-scale NWP model, Quarterly Journal of the Royal Meteorological Society, 142, 2692–2704, https://doi.org/10.1002/qj.2860, 2016.

Chen, F. and Dudhia, J.: Coupling an Advanced Land Surface–Hydrology Model with the Penn State–NCAR MM5 Modeling System. Part I: Model Implementation and Sensitivity, Monthly Weather Review, 129, 569–585, https://doi.org/10.1175/1520-0493(2001)129<0569:CAALSH>2.0.CO;2, 2001.

Cimini, D., Hocking, J., De Angelis, F., Cersosimo, A., Di Paola, F., Gallucci, D., Gentile, S., Geraldi, E., Larosa, S., Nilo, S., Romano, F., Ricciardelli, E., Ripepi, E., Viggiano, M., Luini, L., Riva, C., Marzano, F. S., Martinet, P., Song, Y. Y., Ahn, M. H., and Rosenkranz, P. W.: RTTOV-gb v1.0 – updates on sensors, absorption models, uncertainty, and availability, Geoscientific Model Development, 12, 1833–1845, https://doi.org/10.5194/gmd-12-1833-2019, 2019.

De Angelis, F., Cimini, D., Hocking, J., Martinet, P., and Kneifel, S.: RTTOV-gb – adapting the fast radiative transfer model RTTOV for the assimilation of ground-based microwave radiometer observations, Geoscientific Model Development, 9, 2721–2739, https://doi.org/10.5194/gmd-9-2721-2016, 2016.

De Angelis, F., Cimini, D., Löhnert, U., Caumont, O., Haefele, A., Pospichal, B., Martinet, P., Navas-Guzmán, F., Klein-Baltink, H., Dupont, J.-C., and Hocking, J.: Long-term observations minus background monitoring of ground-based brightness temperatures from a microwave radiometer network, Atmospheric Measurement Techniques, 10, 3947–3961, https://doi.org/10.5194/amt-10-3947-2017, 2017.

Dee, D. P.: Bias and data assimilation, Quarterly Journal of the Royal Meteorological Society, 131, 3323–3343, https://doi.org/10.1256/qj.05.137, 2005.

Eyre, J. R., English, S. J., and Forsythe, M.: Assimilation of satellite data in numerical weather prediction. Part I: The early years, Quarterly Journal of the Royal Meteorological Society, 146, 49–68, https://doi.org/10.1002/qj.3654, 2020.

Eyre, J. R., Bell, W., Cotton, J., English, S. J., Forsythe, M., Healy, S. B., and Pavelin, E. G.: Assimilation of satellite data in numerical weather prediction. Part II: Recent years, Quarterly Journal of the Royal Meteorological Society, 148, 521–556, https://doi.org/10.1002/qj.4228, 2022.

Geer, A. J., Bauer, P., and Lopez, P.: Lessons learnt from the operational 1D + 4D-Var assimilation of rain- and cloud-affected SSM/I observations at ECMWF, Quarterly Journal of the Royal Meteorological Society, 134, 1513–1525, https://doi.org/10.1002/qj.304, 2008.

Geer, A. J., Bauer, P., and Lopez, P.: Direct 4D-Var assimilation of all-sky radiances. Part II: Assessment, Quarterly Journal of the Royal Meteorological Society, 136, 1886–1905, https://doi.org/10.1002/qj.681, 2010.

Geer, A. J., Baordo, F., Bormann, N., Chambon, P., English, S. J., Kazumori, M., Lawrence, H., Lean, P., Lonitz, K., and Lupu, C.: The growing impact of satellite observations sensitive to humidity, cloud and precipitation, Quarterly Journal of the Royal Meteorological Society, 143, 3189–3206, https://doi.org/10.1002/qj.3172, 2017.

Gustafsson, N., Janjić, T., Schraff, C., Leuenberger, D., Weissmann, M., Reich, H., Brousseau, P., Montmerle, T., Wattrelot, E., Bučánek, A., Mile, M., Hamdi, R., Lindskog, M., Barkmeijer, J., Dahlbom, M., Macpherson, B., Ballard, S., Inverarity, G.,

https://doi.org/10.5194/egusphere-2025-12
Preprint. Discussion started: 23 January 2025

Carley, J., Alexander, C., Dowell, D., Liu, S., Ikuta, Y., and Fujita, T.: Survey of data assimilation methods for convective-scale numerical weather prediction at operational centres, Quarterly Journal of the Royal Meteorological Society, 144, 1218–1256, https://doi.org/10.1002/qj.3179, 2018.

Ha, S.-Y. and Snyder, C.: Influence of Surface Observations in Mesoscale Data Assimilation Using an Ensemble Kalman Filter, Monthly Weather Review, 142, 1489–1508, https://doi.org/10.1175/MWR-D-13-00108.1, 2014.

Harris, B. A. and Kelly, G.: A satellite radiance-bias correction scheme for data assimilation, Quarterly Journal of the Royal Meteorological Society, 127, 1453–1468, https://doi.org/10.1002/qj.49712757418, 2001.

Hartung, D. C., Otkin, J. A., Petersen, R. A., Turner, D. D., and Feltz, W. F.: Assimilation of Surface-Based Boundary Layer Profiler Observations during a Cool-Season Weather Event Using an Observing System Simulation Experiment. Part II: Forecast Assessment, Monthly Weather Review, 139, 2327–2346, https://doi.org/10.1175/2011MWR3623.1, 2011.

HE, W., CHEN, H., and LI, J.: Influence of assimilating ground-based microwave radiometer data into the WRF model on precipitation, Atmospheric and Oceanic Science Letters, 13, 107–112, https://doi.org/10.1080/16742834.2019.1709299, 2020.

Hong, S.-Y., Noh, Y., and Dudhia, J.: A New Vertical Diffusion Package with an Explicit Treatment of Entrainment Processes, Monthly Weather Review, 134, 2318–2341, https://doi.org/10.1175/MWR3199.1, 2006.

Iacono, M. J., Delamere, J. S., Mlawer, E. J., Shephard, M. W., Clough, S. A., and Collins, W. D.: Radiative forcing by long-lived greenhouse gases: Calculations with the AER radiative transfer models, Journal of Geophysical Research Atmospheres, 113, undefined-undefined, https://doi.org/10.1029/2008JD009944, 2008.

Kim, M.-J., Jin, J., Akkraoui, A. E., McCarty, W., Todling, R., Gu, W., and Gelaro, R.: The Framework for Assimilating All-Sky GPM Microwave Imager Brightness Temperature Data in the NASA GEOS Data Assimilation System, Monthly Weather Review, 148, 2433–2455, https://doi.org/10.1175/MWR-D-19-0100.1, 2020.

Li, J., Jiang, X., Schiemann, R., Chen, H., Li, Y., and Heng, Z.: Prediction of the Diurnal Variation of Summertime Precipitation Over the Sichuan Basin by a Regional Model, Journal of Geophysical Research: Atmospheres, 128, e2021JD036247, https://doi.org/10.1029/2021JD036247, 2023.

Liu J. J., L. Xu, W. Cheng, B. Wang, X. Y. Gong, Z. R. Deng, Y. Y. Li, and D. Di, 2022. Bias Characteristics and Bias Correction of GIIRS Sounder onboard FY-4A Satellite for Data Assimilation. Chinese Journal of Atmospheric Sciences (in Chinese), 46(2): 275−292. DOI: 10.3878/j.issn.1006-9895.2111.21034

Lin, H.-C., Sun, J., Weckwerth, T. M., Joseph, E., and Kay, J.: Assimilation of New York State Mesonet Surface and Profiler Data for the 21 June 2021 Convective Event, Monthly Weather Review, 151, 485–507, https://doi.org/10.1175/MWR-D-22-0136.1, 2023.

Ma, S., Zhang, W., Cao, X., Zhao, Y., and Liu, B.: Assimilation of All-Sky Radiance from the FY-3 MWHS-2 with the Yinhe 4D-Var System, Journal of Meteorological Research, 36, 750–766, https://doi.org/10.1007/s13351-022-1208-1, 2022.

Martinet, P., Dabas, A., Donier, J.-M., Douffet, T., Garrouste, O., and Guillot, R.: 1D-Var temperature retrievals from microwave radiometer and convective scale model, 67, 27925, https://doi.org/10.3402/tellusa.v67.27925, 2015.

Min, M., Wu, C., Li, C., Liu, H., Xu, N., Wu, X., Chen, L., Wang, F., Sun, F., Qin, D., Wang, X., Li, B., Zheng, Z., Cao, G., and Dong, L.: Developing the science product algorithm testbed for Chinese next-generation geostationary meteorological satellites: Fengyun-4 series, J Meteorol Res, 31, 708–719, https://doi.org/10.1007/s13351-017-6161-z, 2017.

Moker, J. M., Castro, C. L., Arellano, A. F., Serra, Y. L., and Adams, D. K.: Convective-Permitting Hindcast Simulations during the North American Monsoon GPS Transect Experiment 2013: Establishing Baseline Model Performance without Data Assimilation, Journal of Applied Meteorology and Climatology, 57, 1683–1710, https://doi.org/10.1175/JAMC-D-17-0136.1, 2018.

Morrison, H., Thompson, G., and Tatarskii, V.: Impact of Cloud Microphysics on the Development of Trailing Stratiform Precipitation in a Simulated Squall Line: Comparison of One- and Two-Moment Schemes, Monthly Weather Review, 137, 991–1007, https://doi.org/10.1175/2008MWR2556.1, 2009.

Otkin, J. A.: Clear and cloudy sky infrared brightness temperature assimilation using an ensemble Kalman filter, Journal of Geophysical Research: Atmospheres, 115, https://doi.org/10.1029/2009JD013759, 2010.

Otkin, J. A., Hartung, D. C., Turner, D. D., Petersen, R. A., Feltz, W. F., and Janzon, E.: Assimilation of Surface-Based Boundary Layer Profiler Observations during a Cool-Season Weather Event Using an Observing System Simulation Experiment. Part I: Analysis Impact, Monthly Weather Review, 139, 2309–2326, https://doi.org/10.1175/2011MWR3622.1, 2011.

Qi, Y., Fan, S., Mao, J., Li, B., Guo, C., and Zhang, S.: Impact of Assimilating Ground-Based Microwave Radiometer Data on the Precipitation Bifurcation Forecast: A Case Study in Beijing, Atmosphere, 12, 551, https://doi.org/10.3390/atmos12050551, 2021.

Qi, Y., Fan, S., Li, B., Mao, J., and Lin, D.: Assimilation of Ground-Based Microwave Radiometer on Heavy Rainfall Forecast in Beijing, Atmosphere, 13, 74, https://doi.org/10.3390/atmos13010074, 2022.

Saunders, R., Hocking, J., Turner, E., Rayer, P., Rundle, D., Brunel, P., Vidot, J., Roquet, P., Matricardi, M., Geer, A., Bormann, N., and Lupu, C.: An update on the RTTOV fast radiative transfer model (currently at version 12), Geoscientific Model Development, 11, 2717–2737, https://doi.org/10.5194/gmd-11-2717-2018, 2018.

Shen, F., Shu, A., Liu, Z., Li, H., Jiang, L., Zhang, T., and Xu, D.: Assimilating FY-4A AGRI Radiances with a Channel-Sensitive Cloud Detection Scheme for the Analysis and Forecasting of Multiple Typhoons, dqkxjz, 41, 937–958, https://doi.org/10.1007/s00376-023-3072-z, 2024.

Shen, Y., Zhao, P., Pan, Y., and Yu, J.: A high spatiotemporal gauge-satellite merged precipitation analysis over China, Journal of Geophysical Research: Atmospheres, 119, 3063–3075, https://doi.org/10.1002/2013JD020686, 2014.

Shi, Y., Luo, Z., Chen, X., Zhang, Q., Liu, Y., and Liu, C.: Effects of joint assimilation of FY-4A AGRI and ground-based microwave radiometer on heavy rainfall prediction, Front. Environ. Sci., 11, https://doi.org/10.3389/fenvs.2023.1083517, 2023.

Shi, Y.-N., Yang, J., Han, W., Han, L., Mao, J., Kan, W., and Weng, F.: Development of A Fast Radiative Transfer Model for Ground-based Microwave Radiometers (ARMS-gb v1.0): Validation and Comparison to RTTOV-gb, EGUsphere, 1–25, https://doi.org/10.5194/egusphere-2024-2884, 2024.

Shu, T.-T., Han, H.-M., Guo, L.-X., Lin, L.-K., Zhao, Z.-W., and Li, J.-M.: Profiling atmospheric temperature using temperature weighting functions, in: ISAPE2012, ISAPE2012, 1184–1187, https://doi.org/10.1109/ISAPE.2012.6408989, 2012.

Skamarock, C., Klemp, B., Dudhia, J., Gill, O., Liu, Z., Berner, J., Wang, W., Powers, G., Duda, G., Barker, D., and Huang, X.: A Description of the Advanced Research WRF Model Version 4.3, https://doi.org/10.5065/1dfh-6p97, 2021.

https://doi.org/10.5194/egusphere-2025-12
Preprint. Discussion started: 23 January 2025

Su, J., Lü, H., Crow, W. T., Zhu, Y., and Cui, Y.: The Effect of Spatiotemporal Resolution Degradation on the Accuracy of IMERG Products over the Huai River Basin, https://doi.org/10.1175/JHM-D-19-0158.1, 2020.

Sun, W. and Xu, Y.: Assimilation of FY-3D MWHS-2 Radiances with WRF Hybrid-3DVAR System for the Forecast of Heavy Rainfall Evolution Associated with Typhoon Ampil, https://doi.org/10.1175/MWR-D-20-0127.1, 2021.

Vandenberghe, F. and Ware, R.: 4DIMENSIONAL VARIATIONAL ASSIMILATION OF GROUND-BASED MICROWAVE OBSERVATIONS DURING A WINTER FOG EVENT, 2002.

Vural, J., Merker, C., Löffler, M., Leuenberger, D., Schraff, C., Stiller, O., Schomburg, A., Knist, C., Haefele, A., and Hervo, M.: Improving the representation of the atmospheric boundary layer by direct assimilation of ground-based microwave radiometer observations, Quarterly Journal of the Royal Meteorological Society, n/a, https://doi.org/10.1002/qj.4634, 2023.

Wang, D., Wang, X., Liu, L., Wang, D., and Zeng, Z.: Urban Signatures in the Spatial Clustering of Precipitation Extremes over Mainland China, https://doi.org/10.1175/JHM-D-20-0063.1, 2021.

Wei, J., Shi, Y., Ren, Y., Li, Q., Qiao, Z., Cao, J., Ayantobo, O. O., Yin, J., and Wang, G.: Application of Ground-Based Microwave Radiometer in Retrieving Meteorological Characteristics of Tibet Plateau, Remote Sensing, 13, 2527, https://doi.org/10.3390/rs13132527, 2021.

Xia, Y., Chen, J., Du, J., Zhi, X., Wang, J., and Li, X.: A Unified Scheme of Stochastic Physics and Bias Correction in an Ensemble Model to Reduce Both Random and Systematic Errors, https://doi.org/10.1175/WAF-D-19-0032.1, 2019.

Xian, Z., Chen, K., and Zhu, J.: All-Sky Assimilation of the MWHS-2 Observations and Evaluation the Impacts on the Analyses and Forecasts of Binary Typhoons, Journal of Geophysical Research: Atmospheres, 124, 6359–6378, https://doi.org/10.1029/2018JD029658, 2019.

Xu, L., Cheng, W., Deng, Z., Liu, J., Wang, B., Lu, B., Wang, S., and Dong, L.: Assimilation of the FY-4A AGRI Clear-Sky Radiance Data in a Regional Numerical Model and Its Impact on the Forecast of the "21·7" Henan Extremely Persistent Heavy Rainfall, dqkxjz, 40, 920–936, https://doi.org/10.1007/s00376-022-1380-3, 2023.

Yang, L. and Shami, A.: On hyperparameter optimization of machine learning algorithms: Theory and practice, Neurocomputing, 415, 295–316, https://doi.org/10.1016/j.neucom.2020.07.061, 2020.

Yang, Z.-L., Zhao, L., He, Y., and Wang, B.: Perspectives for Tibetan Plateau data assimilation, National Science Review, 7, 495–499, https://doi.org/10.1093/nsr/nwaa014, 2020.

Yin, R., Han, W., Gao, Z., and Di, D.: The evaluation of FY4A's Geostationary Interferometric Infrared Sounder (GIIRS) long-wave temperature sounding channels using the GRAPES global 4D-Var, Quarterly Journal of the Royal Meteorological Society, 146, 1459–1476, https://doi.org/10.1002/qj.3746, 2020.

Yin, R., Han, W., Gao, Z., and Li, J.: Impact of High Temporal Resolution FY-4A Geostationary Interferometric Infrared Sounder (GIIRS) Radiance Measurements on Typhoon Forecasts: Maria (2018) Case With GRAPES Global 4D-Var Assimilation System, Geophysical Research Letters, 48, e2021GL093672, https://doi.org/10.1029/2021GL093672, 2021.

Zhang, X., Xu, D., Li, X., and Shen, F.: Nonlinear Bias Correction of the FY-4A AGRI Infrared Radiance Data Based on the Random Forest, Remote Sensing, 15, 1809, https://doi.org/10.3390/rs15071809, 2023.

https://doi.org/10.5194/egusphere-2025-12
Preprint. Discussion started: 23 January 2025

Zheng, Q., Sun, W., Li, J., Feng, Y., Heng, Z., and Jiang, X.: Impacts of Moisture Advection Scheme on Precipitation in the Steep Topography Region between the Tibetan Plateau and the Sichuan Basin, Journal of Applied Meteorology and Climatology, 63, 781–801, https://doi.org/10.1175/JAMC-D-23-0111.1, 2024.

Zheng, Q., Sun, W., Liu, Z., Mao, J., He, J., Li, J., and Jiang, X.: Code for training the machine learning-based MWR bias correction model, Zenodo [code], https://doi.org/10.5281/zenodo.14586317, 2025a.

Zheng, Q., Sun, W., Liu, Z., Mao, J., He, J., Li, J., and Jiang, X.: Data for manuscript "Direct assimilation of ground-based microwave radiometer observations with machine learning bias correction based on developments of RTTOV-gb v1.0 and WRFDA v4.5", Zenodo [data set], https://doi.org/10.5281/zenodo.14586346, 2025b.